Surface Hardening of Nickel Alloys by Means of Plasma Nitriding

TAKASHI MAKISHI and KAZUHIRO NAKATA

Surface hardening of Ni alloys by plasma nitriding was investigated by using tentative Ni binary alloys contained nitride forming elements such as Ti, Zr, Hf, V, Nb, Ta, Cr, Mo, Mn, Fe, Al, or Si at the nitriding temperature from 673 to 1073 K. Surface hardness was different depending on the types of alloying elements, their contents, and their nitriding temperatures. Higher hardness than HV500 was obtained in Ti, V, Nb, and Cr containing alloys at 823 to 873 K, but other alloys showed lower surface hardness than HV400. The elements Ti, V, Nb, and Cr were the effective alloying elements for the surface hardening of nitrided Ni alloys.

From transmission electron microscopy (TEM) and X-ray diffraction (XRD) analysis, the nitrided layer was composed of fine precipitate particles in the matrix of the nitrided layer. At the lower nitriding temperature, these particles were metastable fine particles or Ginier-Preston (GP) zone having coherency with the matrix, and these fine particles induced large microstrain in the matrix. However, at the higher nitriding temperature, equilibrium nitride particles were precipitated and coherency with the matrix was decreased. Therefore, the hardening of Ni alloys by plasma nitriding was due to the microstrain induced in the nitrided layer by the precipitation of metastable particles or GP.

I. INTRODUCTION

NICKEL and its alloys are widely used as industrial materials, but an industrially available surface hardening process to enhance wear resistance for these materials has not yet been established. In general, there are two types of surface hardening processes, one is a diffusion process such as carburizing, nitriding, or boronizing for iron and steels, and the other is a coating process such as chemical vapor deposition (CVD), physical vapor deposition (PVD), or plating. Among these diffusion processes, boronizing is the only method applicable to surface hardening of Ni and Ni alloys.[1] However, boronizing treatment has not been established as an industrial surface hardening process as have carburizing and nitriding. On the other hand, hard, ceramics coating such as TiN by CVD and PVD is applicable to any metal and alloy, but it is much more costly in comparison with the diffusion process.

On the contrary, the plasma nitriding process, assisted by a glow discharge, is one of the nitriding processes widely used in an industrial surface hardening process due to its beneficial features such as energy and labor savings, good reproducibility of the property of nitrided layer, and no requirement of antipollution equipment.[2] Therefore, the plasma nitriding process is applied not only to iron and steels but also to nonferrous metals such as titanium, zirconium, *etc.*[3]

However, the nitriding treatment has not been applied to Ni, because metals such as Ni, Co, Cu, Au, and Ag, which do not have the solubility of nitrogen and no stable nitride, cannot be hardened by nitriding treatment.

It is well known that the typical nitride forming elements of IVa, Va, and VIa families in the periodic table are easily hardened by nitriding treatment. This suggests when some nitriding forming elements are alloyed to pure nickel, surface hardening of Ni alloy by nitriding may become possible. At the nitriding process, the nitrogen diffuses into Ni alloy from its surface and reacts with alloying elements to make their nitrides, and this will form the hardened layer on the surface of Ni alloy.

Therefore, in this article, the probability of surface hardening of Ni alloy by means of the plasma nitriding process has been investigated. The individual effect of nitride forming elements on surface hardening of Ni alloys has been investigated by using tentative Ni binary alloys, and a beneficial alloying element and its effective content for surface hardening of Ni alloy have been examined. Moreover, the surface hardening mechanism of nitrided Ni alloys has been discussed mainly using transmission electron microscopy (TEM), X-ray diffraction (XRD) analysis, and electron probe microanalysis.

II. EXPERIMENTAL PROCEDURES

A. *Material Used*

Thirty-one types of tentative Ni binary alloys, which contained nitride forming elements of Ti, V, Nb, Ta, Cr, Mo, Mn, Fe, Al, and Si up to the solubility limit for each element, were prepared with high frequency induction melting in an argon atmosphere.[4] These alloys were rolled at 1273 K after casting and then annealed at 1173 K for 10.8 ks. Chemical compositions of these alloys are shown in Table I, where each base metal hardness after plasma nitriding was also shown. In addition, eight types of commercially used Ni alloys were also used for comparison, of which chemical compositions are shown in Table II.

Specimen size for plasma nitriding was 10 mm width × 20 mm length × 3 mm thickness. A specimen surface was polished by emery paper up to No. 1200 and degreased with acetone before nitriding.

TAKASHI MAKISHI, Associate Professor, is with the Department of Mechanical Systems Engineering, University of Ryukyus, Okinawa 903-0213, Japan. Contact e-mail: makishi@tec.u-ryukyu.ac.jp KAZUHIRO NAKATA, Professor, is with the Joining and Welding Research Institute, Osaka University, Osaka 567-0047, Japan.

Manuscript submitted September 24, 2002.

Table I. Chemical Composition of Tentative Nickel Binary Alloys

Alloying Element	Alloy	Content of Alloying Element (Mass Pct)	Hardness (HV)	Solid Solubility in Ni (Mass Pct) (Temperature)
Ti	1Ti	1.10	130	7 (873 K)
	1.5Ti	1.56	130	
	4Ti	3.69	150	
	7Ti	7.19	180	
Zr	0.3Zr	0.23	120	0.5 (293 K)
Hf	1Hf	0.76	125	<0.5
V	1V	1.01	130	15 (873 K)
	5V	5.01	150	
	10V	9.87	180	
	15V	14.87	260	
Nb	1Nb	1.25	140	9 (1073 K)
	4Nb	3.89	170	
	10Nb	9.97	200	
Ta	1Ta	0.98	130	4 (873 K)
	3Ta	2.86	140	
	5Ta	4.97	160	
Cr	5Cr	5.29	130	32 (823 K)
	10Cr	10.60	140	
	15Cr	15.10	140	
	20Cr	20.54	150	
	30Cr	29.15	160	
Mo	5Mo	4.86	150	22 (873 K)
	10Mo	9.89	170	
	20Mo	17.70	190	
Mn	10Mn	10.07	140	38 (873 K)
	30Mn	29.70	170	
Fe	10Fe	10.41	130	74 (873 K)
	20Fe	20.82	140	
	30Fe	33.12	160	
Al	6Al	5.68	170	7 (1073 K)
Si	5Si	4.86	150	5 (873 K)

Table II. Chemical Composition of Commercially Used Ni Alloys and Pure Ni

Alloy	Chemical Composition (Mass Pct)
INCONEL 600	Ni-0. 04C-0. 2Si-15. 8Cr-7. 2Fe
INCONEL 625	Ni-0. 02C-0. 2Mn-0. 4Si-21. 6Cr-8.3Mo-3.7Nb-2. 6Fe-0. 2Ti-0. 1Al
INCONEL 713C	Ni-0. 12C-12. 5Cr-4. 2Mo-2. 0Nb-2.5Fe-0.8Ti-6. 1Al-0. 1Zr
Udimet 500	Ni-0. 09C-18. 8Cr-16. 7Co-3. 5Mo-0.2Fe-3.0Ti-3. 0Al
Hastelloy B	Ni-0. 01Cr-0. 8Co-27. 0Mo-4. 8Fe-0. 03V
Hastelloy C	Ni-15. 5Cr-16.0Mo-5. 5Fe
Hastelloy G	Ni-22. 0Cr-6. 5Mo-2. 0Nb-19. 5Fe-2.0Cu-4.0W
Permalloy	Ni-0. 1Co-4. 3Mo-15. 5Fe
Pure nickel	99. 96Ni

*INCONEL is a trademark of INCO alloys International, Toronto, ON, Canada.

Hastelloy is a trademark of Haynes International Inc., Kokomo, IN.

Udimet is a trademark of Special Metal Corp., Huntington, WV.

Permalloy is a trademark of B&D Industrial & Mining Services Inc., Jasper, AL.

B. *Plasma Nitriding Process*

Figure 1 shows a schematic illustration of the plasma nitriding apparatus and specimen arrangement used in this experiment. A specimen is set on a cathode plate, which is made of pure nickel in a vacuum chamber. The direct current (DC) glow discharge between a vacuum chamber wall as anode and a specimen as cathode was used for nitriding treatment. After the vacuum chamber was evacuated to a pressure of about 0.65 Pa by mechanical pump, nitrogen and hydrogen mixed gas (nominal gas purity 99.9999 pct, mixed ratio: 50 vol pct N_2 + 50 vol pct H_2) was fed into the vacuum chamber up to a constant pressure at 800 Pa.

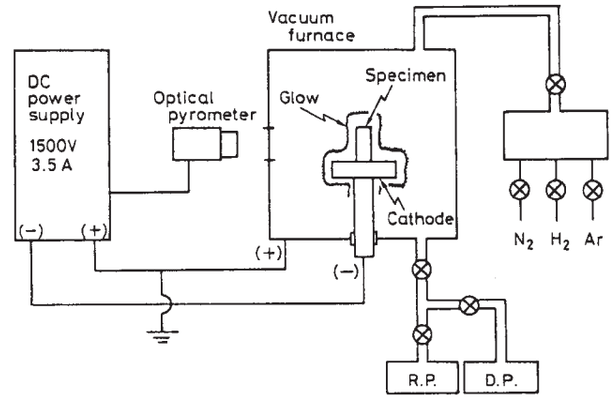

Fig. 1—Schematic illustration of experimental apparatus for plasma nitriding.

The nitriding temperature, which was the specimen surface temperature measured by an optical pyrometer, was kept constant by controlling the discharge power, and varied from 673 to 1073 K. The heating rate was about 40 K/min, and the cooling rate was about 70 K/min from each nitriding temperature to 573 K after nitriding. The nitriding time was varied from 3.6 to 32.4 ks.

C. *Characterization of the Nitrided Specimen*

After nitriding, surface hardness of each specimen was measured by using a microvickers hardness tester with a 0.1 N load. The cross section of each specimen was observed by using optical microscopy after electrolytic etching using 10 pct oxalic acid solution. The compositions of alloying elements and nitrogen in the nitrided layer were determined by means of an electron probe microanalyzer (EPMA), and the type of nitride was identified by XRD analysis with Cu K_α radiation at 40 kV, 20 mA. Moreover, the microstructure of the nitrided layer was observed using TEM. Figure 2 shows the schematic illustration preparing the specimen for TEM. The TEM specimens were cut off from the nitrided specimen, and mechanically polished to 100 μm in thickness, and then polished electrolytically from the opposite surface of the specimen to the nitrided layer surface using a standard jet electrolytic polishing technique. The nitrided surface was coated with polystyrene solution for protection. The electrolyte consists of 23 parts of 70 pct perchloric acid and 77 parts of acetic acid about 288 K. The polishing voltage was 15 V.

III. RESULTS AND DISCUSSION

A. *Effect of Alloying Element on Surface Hardening*

Figure 3 shows the relation between surface hardness and nitriding temperature for tentative Ni alloys containing the

maximum content of alloying element. The core hardness after plasma nitriding was in the same range of each base metal hardness and not varied by plasma nitriding at nitriding conditions used in this study.

Remarkable surface hardening was observed on 7Ti, 30Cr, 15V, and 10Nb at nitriding temperatures of 673 to 1073 K and nitriding times of more than 10.8 ks. The surface hardness of these alloys increased with increasing nitriding temperature from 673 to 823 or 873 K, and showed the maximum surface hardness at 800 to 900 K for each alloy, and then decreased with increasing nitriding temperature more than 923 K. The maximum surface hardness for each alloy was approximately HV750 to 800 for 7Ti and 30Cr, HV690 for 15V, and HV550 for 10 Nb. 20Mo, 30Fe, and 5Ta were hardened, but their maximum hardnesses, HV350, 320, and 300, respectively, were lower than the preceding alloys. 5Si, 6Al, and 30Mn were slightly hardened as HV200 to 300. From these results, it is confirmed that Ni binary alloys containing nitride former could be hardened by plasma nitriding.

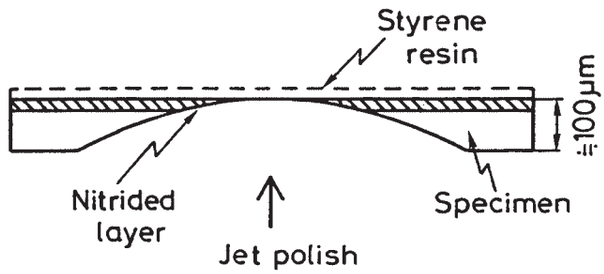

Fig. 2—Schematic illustration of specimen for TEM obseration.

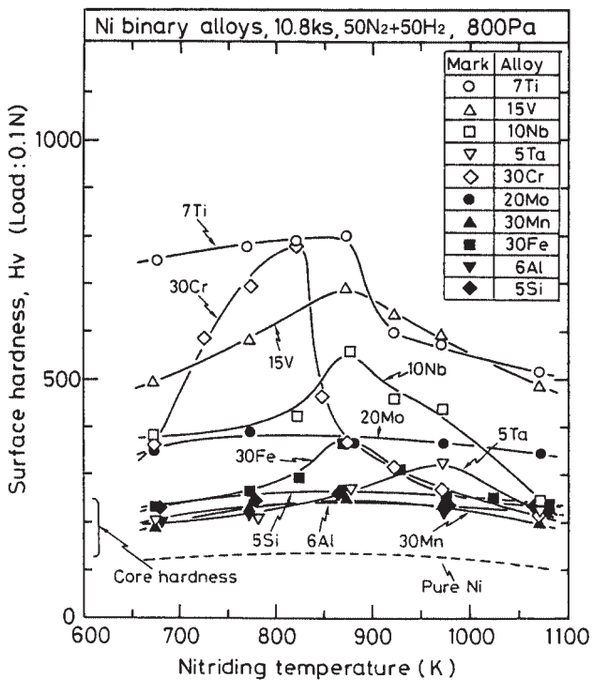

Fig. 3—Relation between surface hardness and nitriding temperature for Ni binary alloys.

Figure 4 shows the relation between the maximum surface hardness and the content of alloying element after plasma nitriding. Hardness of Ni in Figure 4 is the surface hardness of pure nickel after plasma nitriding, about Hv130. The surface hardness was much different, depending on the type of alloying element and its content. A linear relationship was obtained between surface hardness and the alloying content for each alloy system. A gradient of each line in Figure 4 represents a hardness increasing rate to the alloying content, (ΔHv)/(the maximum alloy content (mass pct)); ΔHv = (maximum hardness) − (surface hardness of pure nickel after plasma nitriding), which means the hardenability of each alloying element in nickel at plasma nitriding. These values obtained for each alloying element were as follows: Ti, 100; Nb, 50; V, 40; Ta, 30; Al, 25; Cr, 20; Si, 15; Mo, 10; Fe, 7; Mn, 4. The most effective element for surface hardening of Ni alloy was the IVa family in the periodic table, and followed in order by Va, (VIa, IIIb, IVb), and (VIIa, VIII) families. Judging from the hardness increasing rate and the maximum surface hardness, Ti, V, Nb, and Cr are the most effective alloying element for the surface hardening of Ni alloy by plasma nitriding. On the contrary, it is considered that (Ta, Al) and (Mo, Fe, Mn) are not effective, because the former two elements have low solid solubility in nickel; therefore, these alloys showed low surface hardness, and the latter three elements show low hardness increasing rate.

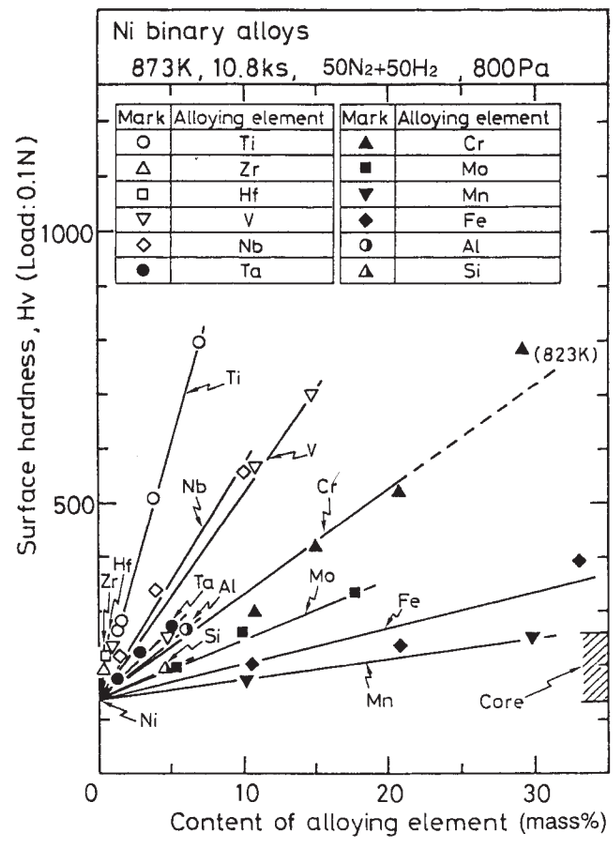

Fig. 4—Effect of alloying content on surface hardness of Ni binary alloys after plasma nitriding.

B. *Estimation of Surface Hardness of Commercially Used Ni Alloys after Plasma Nitriding*

By using the hardness increasing rate obtained from Figure 4, an equation for estimating the surface hardness of Ni alloys after plasma nitriding was drawn as Eq. [1] on the assumption that the effect of each alloying element on the surface hardness can be additive without mutual effect.

$$\begin{aligned}(\text{Hvs})\,E = {} & 100\,(\text{Ti}) + 50\,(\text{Nb}) + 40\,(\text{V}) + 30\,(\text{Ta}) \\ & + 25\,(\text{Al}) + 20\,(\text{Cr}) + 15\,(\text{Si}) + 10\,(\text{Mo}) \\ & + 7\,(\text{Fe}) + 4\,(\text{Mn}) + 130\ (\pm 15\ \text{pct}) \quad [1]\end{aligned}$$

where

(Hvs) E = estimated surface hardness by Eq. [1];
(element) = content of alloying element in mass pct;
numerical coefficients = hardness increasing rate of each alloy;
130 of last term = the surface hardness of pure nickel after plasma nitriding; and
the value of (±15 pct) = hardness allowance.

Equation [1] should be applied to estimate the surface hardness under the conditions of nitriding temperature at 873 K, nitriding time for 10.8 ks, and treated gas with 50 vol pct N_2 + 50 Vol pct H_2 at 800 Pa gas pressure.

The applicability of Eq. [1] was examined by using the data measured on eight types of commercially used Ni alloys after plasma nitriding. Figure 5 shows the relation between the surface hardness estimated by Eq. [1] and the surface hardness measured. The range between two solid lines in Figure 5 is the applicable range of Eq. [1] (±15 pct). As a result, there was good agreement between the hardness estimated and the hardness measured, although the hardness measured of INCONEL 600 and 713C was shown to be slightly higher than the hardness estimated. Consequently, Eq. [1] is applicable to estimate the surface hardness after plasma nitriding for Ni alloys that complexly contained various alloying elements.

C. *Effect of Alloying Element on Formation of Nitrided Layer*

Figure 6 shows the typical microphotographs of the nitrided layer by electrolyte etched with 10 pct oxalic acid solution on the cross section of Ni binary alloys containing the maximum content of the alloying element. A nitrided layer was clearly observed in Ni-Ti, -V, -Nb, and -Cr binary alloys, and there were two types of nitrided layer: one was a single layer as observed on Ni-Ti and -Nb alloys, and the other was a double layer as observed on Ni-V and -Cr alloys. On the contrary, the nitrided layer was not observed in Ni-Ta, -Mo, -Mn, -Fe, -Al, and -Si alloys, but grain boundaries near the specimen surface appeared in these alloys as observed in the Ni-Mo alloy. Moreover, these grain boundaries were also observed in the nitrided layers on Ni-V, -Nb, and -Cr alloys. From the result of microstructural observation, it is made clear that the Ni alloy with the obvious nitrided layer showed remarkable

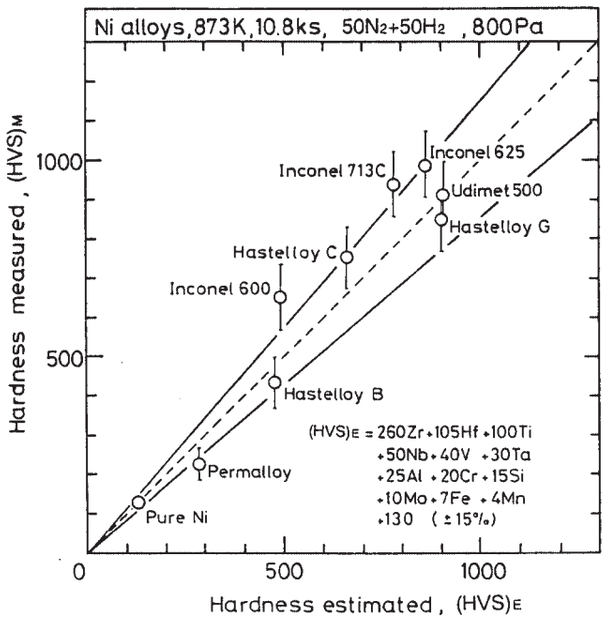

Fig. 5—Relation between hardness estimated (HVs) E and hardness measured (HVs) M for commercially used Ni alloys.

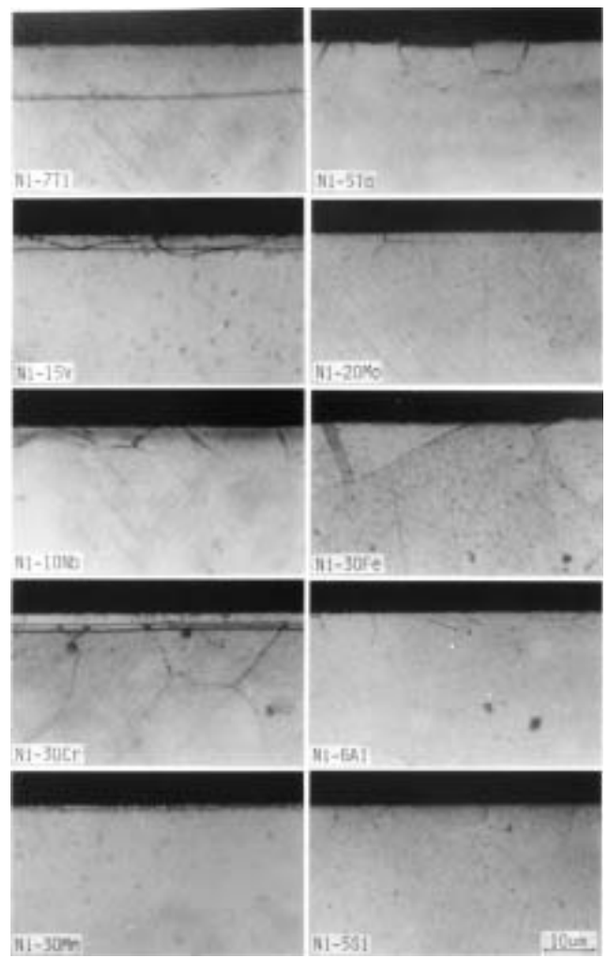

Fig. 6—Micrographs on cross section of Ni binary alloys after plasma nitriding at 873 K for 10.8 ks.

surface hardening by plasma nitriding, and on the contrary, the alloys with no nitrided layer were slightly hardened. Neither the cause for the single layer in Ni-Ti and Ni-Nb alloys nor the double layer in Ni-V and Ni-Cr alloys is clear. It is considered that these differences of nitrided layers are caused by solid solubility of nitrogen and the tendency of formation of each nitride in each alloy. The formation and growth mechanism of the nitrided layer by plasma-nitrided Ni alloys will be described in a future article.

Figure 7 shows the relation between the thickness of the nitrided layer and the content of the alloying element in Ni-Ti, -V, -Nb, and -Cr alloys. The nitrided layer was observed with alloying contents greater than 4, 4, 10, and 10 mass pct for Ni-Ti, -V, -Nb, and -Cr alloys, respectively. The thickness of the nitrided layer of Ni-Ti alloys increased linearly with increasing Ti content, and was much thicker than those for the other alloy systems. The maximum thickness of the nitrided layer was about 12 μm at the maximum content of Ti. Those of Ni-V, -Nb, and -Cr alloy systems increased also with increasing alloy content, but they were likely to saturate to about 3 to 5 μm even with the maximum content near the limit of the solid solubility in nickel for each element. Consequently, Ti was the most effective alloying element for surface hardening by plasma nitriding to make a thick and hard nitrided layer.

In order to examine the composition of the nitrided layer, nitrogen and each alloying element were analyzed with EPMA. Figure 8 shows the typical results of EPMA for Ni-7Ti and -30Cr alloys, which were the typical alloys showing single and double nitrided layers, respectively,

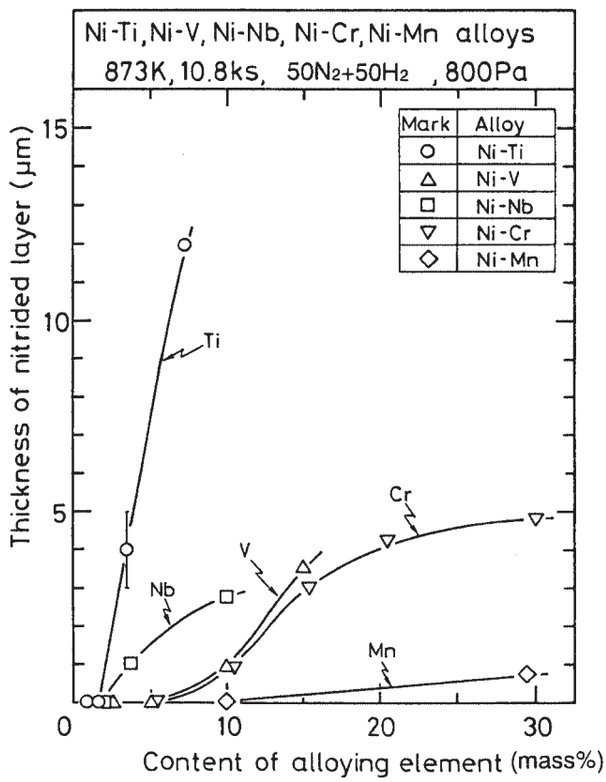

Fig. 7—Effect of alloying content on thickness of nitrided layer.

and -20Mo, which showed no nitrided layer. Nickel was electrolytic plated on the specimen surface to protect the surface detail.

The EPMA results revealed that nitrogen concentrated only in the nitrided layer. The distribution of nitrogen in the nitrided layer of Ni-7Ti was almost constant through the nitrided layer. In Ni-30Cr showing double layer, nitrogen concentration in the nitrided layer was not uniform, and nitrogen content in the outer layer was higher than in the inner layer. On the contrary, there was no difference in the contents of Ni and each alloying element, Ti or Cr, between the nitrided layer and base metal. The similar distributions of nitrogen and alloying elements were observed in the nitrided layers of Ni-V and -Nb alloys. Inversely, for Ni-20Mo, only a slight concentration of nitrogen near the surface of the specimen was observed.

These results suggest that the nitrided layer is not a compound layer of the nitride only, because the nickel does not form a stable nitride. Therefore, the nitrided layer might be a layer in which the nitride of the alloying element precipitated dispersively in the layer matrix or nitrogen concentrated as a solid solution in the layer. The microstructure of the nitrided layer is discussed in Section D.

D. *TEM Microstructure of Nitrided Layer*

Figures 9 and 10 show the typical TEM microphotographs and diffraction patterns of the nitrided layers of Ni-7Ti and -30Cr treated at 723 to 1073 K. Many fine particles were observed in the nitrided layer at each nitriding temperature. Particle size increased with an increase in the nitriding temperature. In the case of the Ni-7Ti alloy at 723 K, particle size was about 6 nm and the shape was disklike, but at 1073 K, particle size increased to 10 to 15 nm and the shape changed to spheroid. Moreover, the number of particles per unit area, particle density, decreased with the increase of nitriding temperature. Namely, particle density was about $6 \times 10^{22}/m^3$ at 723 K, but decreased to about $2.4 \times 10^{22}/m^3$ at 1073 K. In Ni-30Cr, a similar change occurred.

Only diffraction spots of Ni (γ) as the matrix of the nitrided layer were identified at 723 and 873 K in Ni-7Ti and at 723 K in Ni-30Cr, but the diffraction spots of any nitride were not

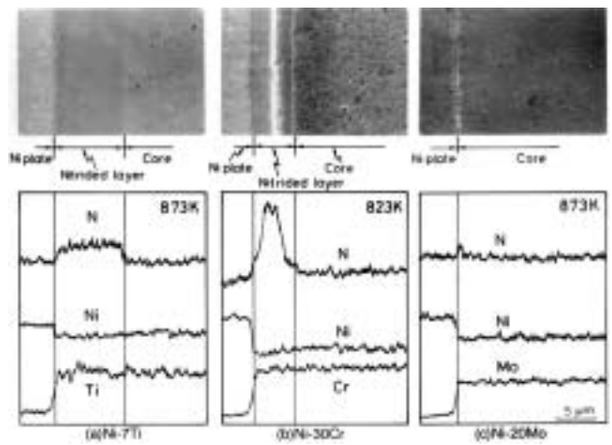

Fig. 8—Distribution of N, Ni, and alloying elements in the nitrided layer for Ni-7Ti, 30Cr, and 20Mo nitrided at 873 K for 10.8 ks.

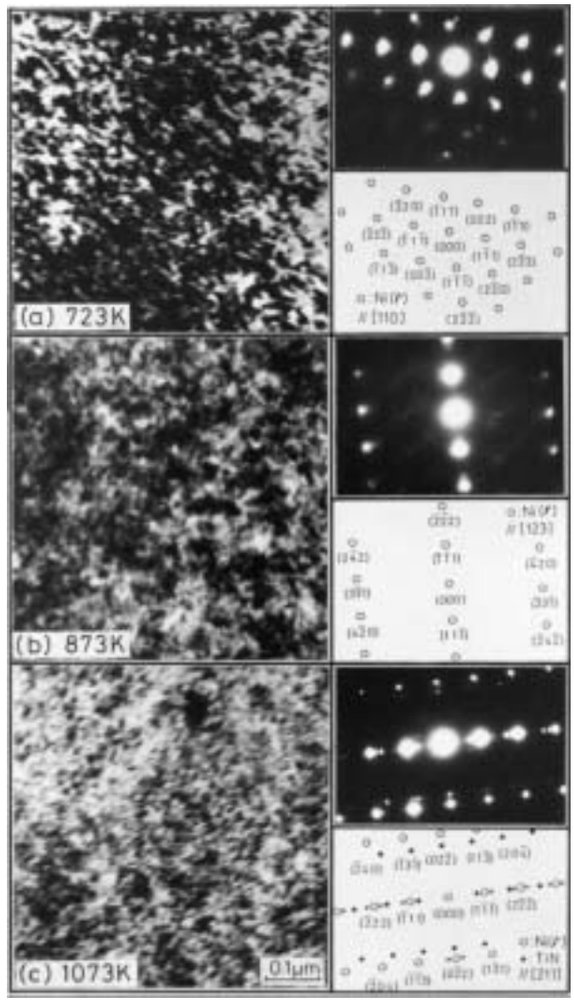

Fig. 9—Electron micrographs and diffraction patterns of Ni-7Ti nitrided at (*a*) 723 K, (*b*) 873 K, and (*c*) 1073 K.

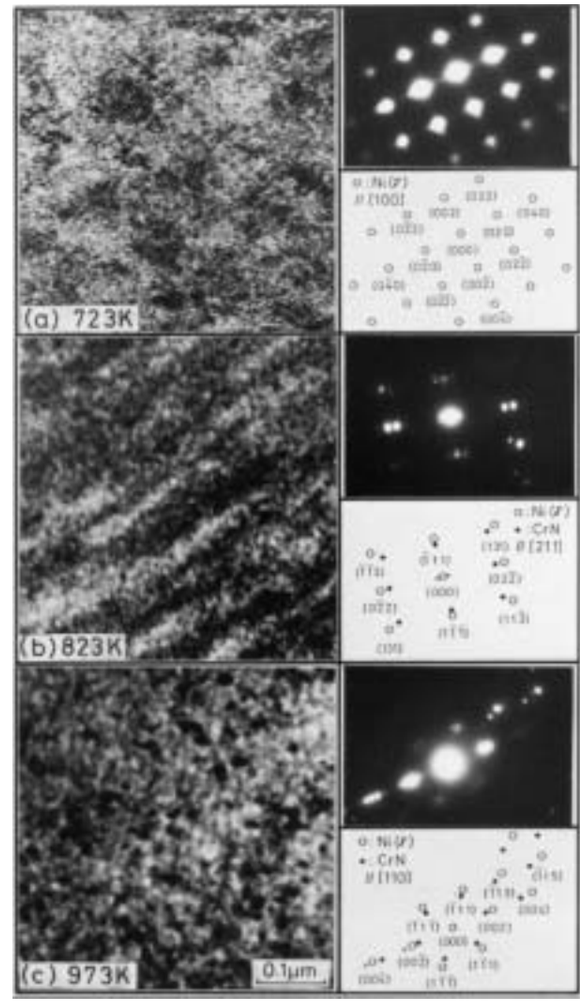

Fig. 10—Electron micrographs and diffraction patterns of Ni-30Cr nitrided at (*a*) 723 K, (*b*) 823 K, and (*c*) 973 K.

detected at these low nitriding temperatures in spite of the existence of many fine particles. Therefore, the fine particles formed at these temperature were not identified.

However, the shape of these diffraction spots was diffused, and in addition, the streaks were observed at 723 K, but not observed at temperatures higher than 823 K. These phenomena indicate that very fine particles having coherency with the matrix such as the Ginier-Preston (GP) zone precipitated and a large microstrain was induced in the nitrided layer at the low nitriding temperature.

On the contrary, at high nitriding temperature, TiN as the nitride in Ni-7Ti at 1073 K and CrN as the nitride in Ni-30Cr at 823 K and 973 K were identified together with Ni (γ) as the matrix. From diffraction spot analysis at these temperatures, each lattice plane of the nitride particle was parallel to the Ni (γ) matrix and the nitride particles precipitated parallel to the $<100>$ direction of the Ni (γ) matrix. Moreover, the double diffraction phenomena were observed in the diffraction spot of Ni (γ) and the nitride, because two phases coexisted in the same diffraction area.[5]

At nitriding temperatures higher than 973 K for Ni-7Ti and 873 K for Ni-30Cr, each diffraction spot became small and sharp, and the streak disappeared. These changes mean that the nitrides became coarse and decreased the coherency with the matrix. Thus, the microstrain of the nitrided layer decreased at high nitriding temperature.

Similar TEM microstructures and the diffraction patterns were observed in Ni-15V and -10Nb alloys, as shown in Figure 11. The fine particles were identified to be VN and NbN as the nitride, respectively, as well as Ni (γ) matrix. The shape of the nitride in 15V and 10Nb was spherical. Each lattice plane of these nitrides was also parallel to the matrix of Ni (γ), and those diffraction spots also showed double diffraction. Moreover, coarsening of nitride particles and decreasing of particle precipitation density occurred with increasing nitride temperature.

Upon review of the results of TEM observation and diffraction pattern analysis, it is clear that these nitrided layers formed by plasma nitriding were the nitrided dispersed–precipitation layer caused by the internal nitriding mechanism,

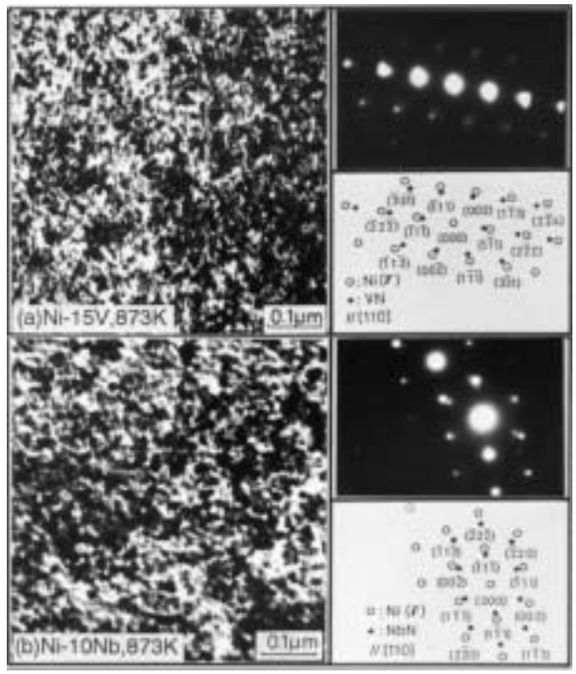

Fig. 11—Electron micrographs and diffraction patterns of (*a*) Ni-15V and (*b*) Ni-10Nb nitrided at 873 K.

that is, nitrogen diffused inward toward the matrix from the surface and combined with the alloying element there to form nitrides or metastable particles as precipitates at high or low nitriding temperature, respectively.

Figure 12 shows the relationships between the density and the size of precipitation particles and nitriding temperature. The size of particles means the diameter of particles measured in TEM micrographs. These data of 15V and 10Nb at lower than 850 K were not obtained, because the nitrided layer of these alloys was too thin to prepare the specimen for TEM observation. With increasing nitriding temperature, the particle size increased, but the precipitation density of particles decreased irrespective of the alloy. Compared with the size and density of particles of each alloy, the finest size and the largest precipitation density of particles were obtained at 7Ti, and 15V, 10Nb, and 30Cr followed in order, except at 723 K.

E. *XRD Analysis*

Figure 13 and 14 show the results of XRD analysis from the specimen surface of Ni-7 Ti and -30 Cr nitrided layers at the nitriding temperatures from 723 to 1073 K. In addition, Figure 15 shows the typical XRD pattern from the specimen surface of Ni-30 Fe after nitriding as the example of the alloy that formed no nitrided layer. The phases identified by XRD analysis for all Ni binary alloys nitrided at 873 K are listed in Table III, which, in addition, shows whether the nitrided layer was formed, as mentioned in Figure 6.

Three typical types of diffraction peaks were observed in these analyses. One is shown as γ in figures from the substrate base metal beneath the nitrided layer, and these peaks were sharp. The second type is from the nitride of each alloying element. Nitrides were identified in Ni-Ti, -V,

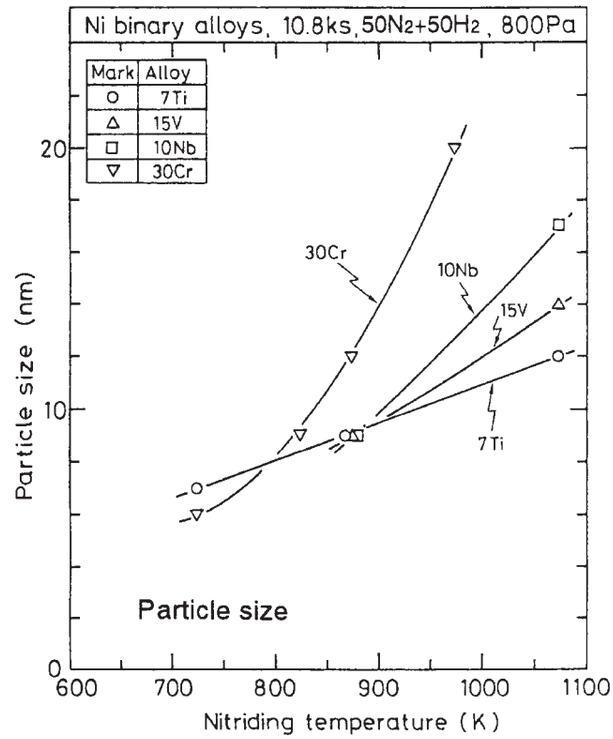

(*a*)

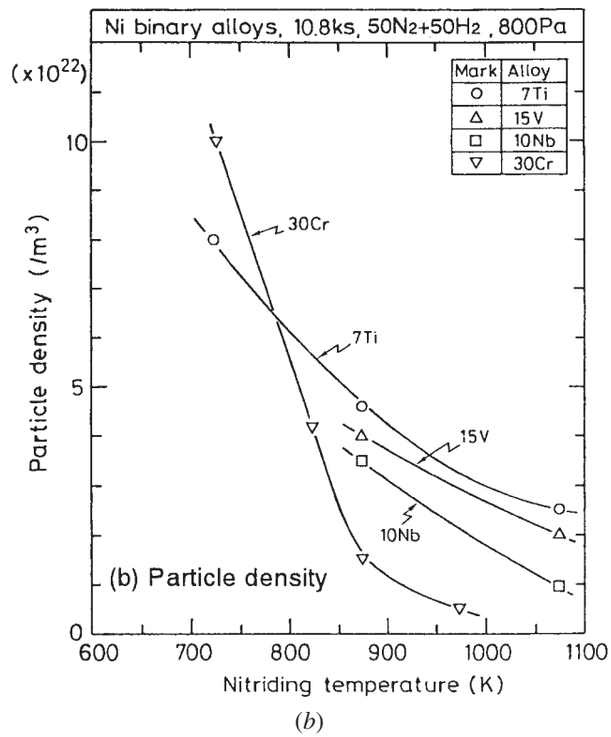

(*b*)

Fig. 12—Effect of nitriding temperature on precipitation particle size and density in nitrided layer: (*a*) particle size and (*b*) particle density.

-Nb, -Cr, -Mo, -Mn, -Fe, and -Al alloys with alloying contents greater than 4, 10, 4, 10, 20, 10, 10, and 6 mass pct, respectively, but was not identified in Ni-Ta and -Si alloys.

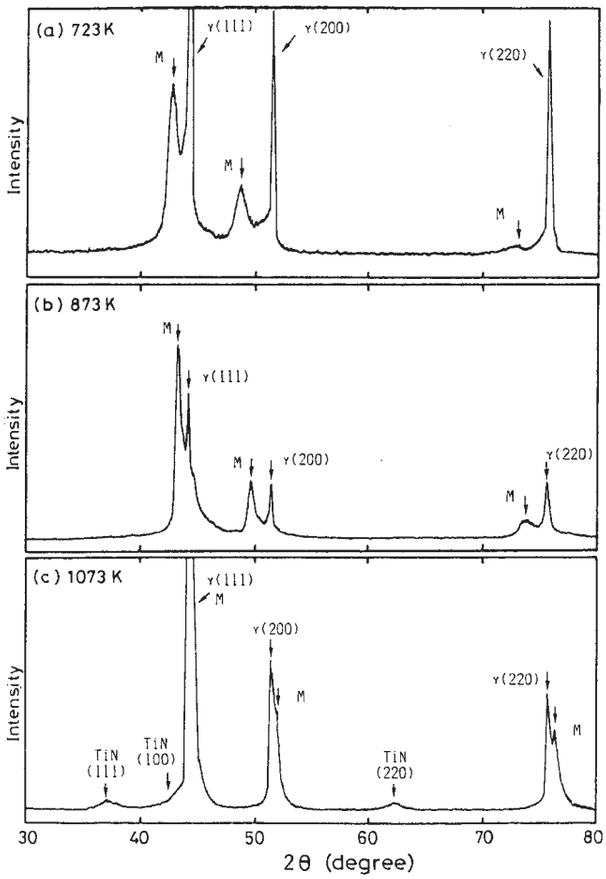

Fig. 13—XRD pattern of the surface of specimen after plasma nitriding of Ni-7Ti at (a) 723 K, (b) 873 K, and (c) 1073 K.

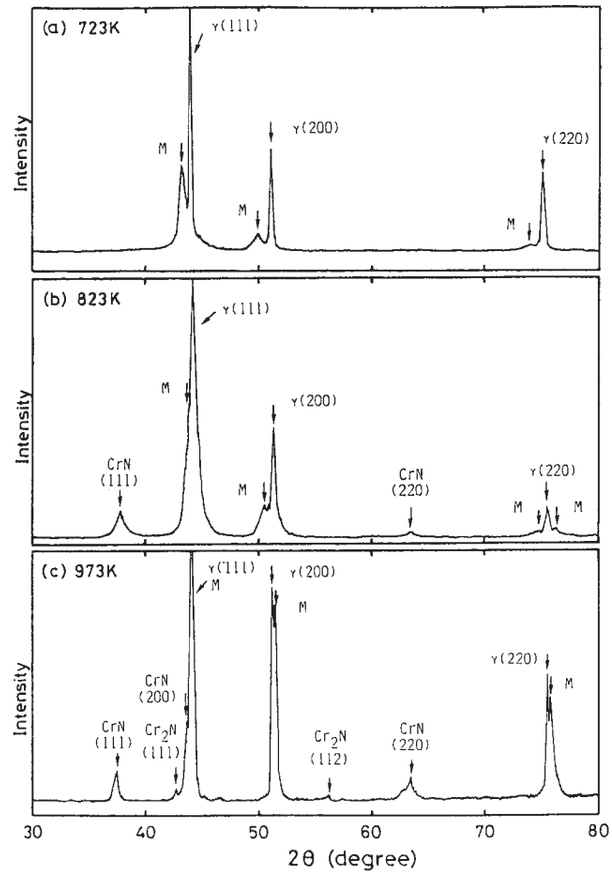

Fig. 14—XRD pattern of the surface of the specimen after plasma nitriding of Ni-30Cr at (*a*) 723 K, (*b*) 823 K, and (*c*) 973 K.

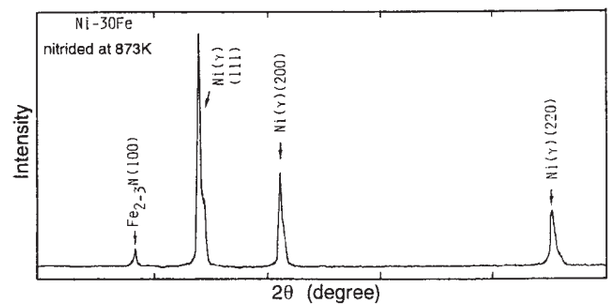

Fig. 15—XRD pattern of the surface of specimen after plasma nitriding of Ni-30Fe at 873 K.

Judging from the free energy of the formation of the nitride of each alloying element, the nitrides of Ta and Si should be formed at these nitriding temperature.[6] The reason why these nitrides were not detected was considered to be that the amount of the nitride precipitated was too little to be detected by XRD.

Moreover, the third is shown as M in Figures 13 and 14 and Table III, which observed near each peak of the base metal γ. The M phase was not detected in the ASTM Powder Diffraction File. A close relationship was observed between the M phase and the formation of the nitrided layer. It was identified only in the alloys with the obvious nitrided layer in Ni-Ti, -V, -Nb, -Cr, and -Mn alloy systems, but not identified in the alloys with no nitrided layer. Moreover, one peak of the M phase corresponded to each peak of Ni (γ) in the alloy showing the single nitrided layer such as Ni-Ti alloy in Figure 13. In addition, in the case of the alloys showing the double nitrided layer such as Ni-Cr alloy in Figure 14 two diffraction peaks of M phase were observed corresponding to each peak of Ni (γ). Therefore, the crystal structure of the M phase was the same as that of the base metal of each alloy. As mentioned, EPMA analysis and TEM observation suggested that the nitrided layer was composed of fine particles precipitated in the layer matrix. Therefore, these results of EPMA, TEM, and XRD analyses indicate that the M phase is the matrix of the nitrided layer in which fine nitride particles or metastable particles precipitate dispersively. The term M is the matrix of the nitrided layer, where nitride or metastable particle precipitated.

In the Ni-Cr alloys, the chromium nitride Cr_2N was detected at high nitriding temperature by XRD analysis. But it was not detected by TEM observation at the same nitride condition because the observation area of TEM was restricted to the surface of the nitrided layer, as explained in Section II–C. This, however, indicated that Cr_2N was formed in the inner nitrided layer, and the outer layer included CrN precipitation.

Table III. Results of XRD Analysis of Ni Binary Alloys after Plasma Nitriding at 873 K

Alloy	Identified Phase			Nitrided Layer*
	Vs	s	w	
1Ti	Ni (γ)	—	—	x
1.5Ti	Ni (γ)	—	—	x
4Ti	Ni (γ)	M	TiN	o
7Ti	M	Ni (γ)	TiN	o
0.3Zr	Ni (γ)	—	—	x
1Hf	Ni (γ)	—	—	x
1V	Ni (γ)	—	—	x
5V	Ni (γ)	—	—	x
10V	Ni (γ)	M	VN	o
15V	Ni (γ)	M	VN	o
1Nb	Ni (γ)	—	—	x
4Nb	Ni (γ)	M	NbN	o
10Nb	Ni (γ)	M	NbN, Nb_3N_4	o
1Ta	Ni (γ)	—	—	x
3Ta	Ni (γ)	—	—	x
5Ta	Ni (γ)	—	—	x
5Cr	Ni (γ)	—	—	x
10Cr	Ni (γ)	M	CrN	o
15Cr	Ni (γ)	M	CrN	o
20Cr	Ni (γ)	M	CrN	o
30Cr	Ni (γ)	M	CrN	o
5Mo	Ni (γ)	—	—	x
10No	Ni (γ)	—	—	x
20No	Ni (γ)	—	MoN	x
10Mn	Ni (γ)	—	Mn_4N	x
30Mn	Ni (γ)	M	Mn_4N	o
10Fe	Ni (γ)	—	$Fe_{2-3}N$	x
20Fe	Ni (γ)	—	$Fe_{2-3}N$	x
30Fe	Ni (γ)	—	$Fe_{2-3}N$	x
6Al	Ni (γ)	—	AlN	x
5Si	Ni (γ)	—	—	x

*o: observed, x: not observed, vs: very strong, s: strong, and w: weak.

As to the typical two features of the M phase, broadening and shift of diffraction peaks against nitriding temperature were observed, which closely related to surface hardening. The broadening of the width of diffraction peaks of M phase as well as nitrides was observed in the alloys that showed high surface hardness at low nitriding temperature, but the width of these diffraction peaks became sharp at high nitriding temperatures, which showed lower surface hardness. These suggested that the microstrain in the M phase was changed by nitriding temperature.

In general, the broadening of the diffraction peak is caused by the microstrain of the lattice.[7] Figure 16 shows the relation between nitriding temperature and the half value width of the diffraction peaks M in Ni-Ti, -V, -Nb, and -Cr alloys.

The half value width of M peaks was selected from the peaks beside $\gamma(220)$. The half value width of M phase decreased linearly with increasing nitriding temperature. These mean that the microstrain induced in the matrix of the nitrided layer decreased with increasing nitriding temperature.

The surface hardness of the alloys with the obvious nitrided layer, Ni-Ti, -V, -Nb, and -Cr alloys, is shown in Figure 17 as the function of the half value width of the M peak. There was a close relationship between the surface hardness and the half value width. Surface hardness increased linearly with the increase in the half value width of the M peak. Therefore,

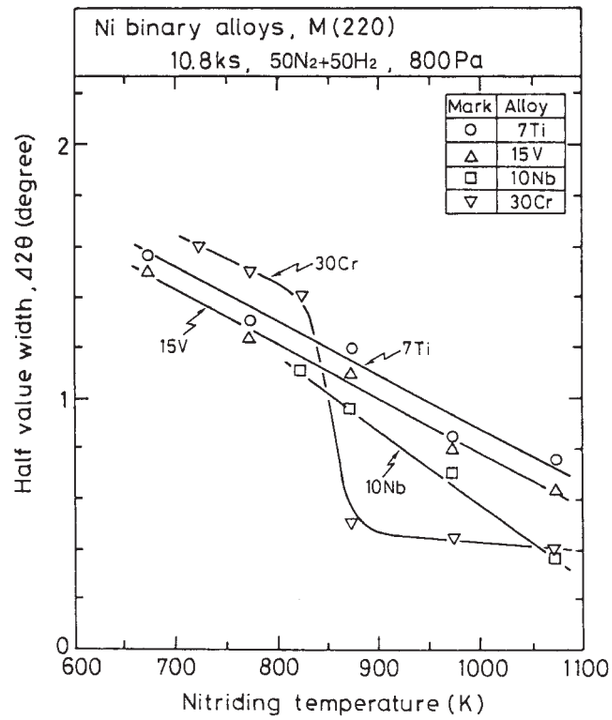

Fig. 16—Effect of nitriding temperature on the half value width of XRD (220) of the matrix of the nitrided layer.

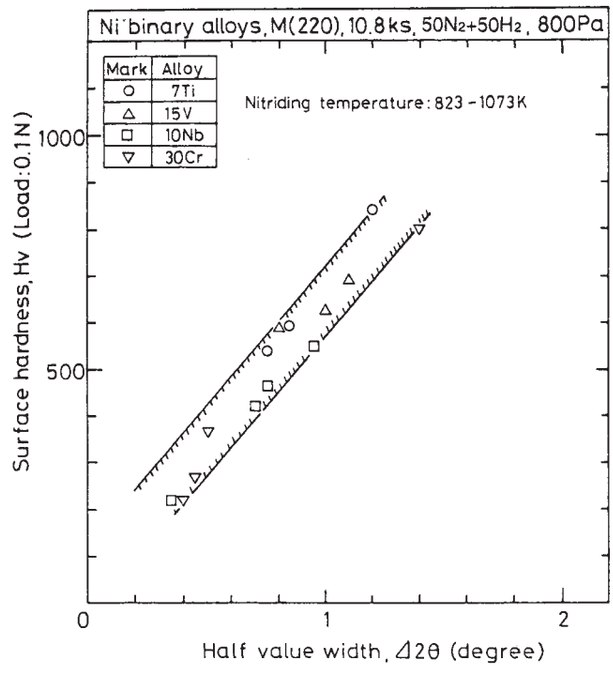

Fig. 17—Relation between surface hardness and the half value width of XRD (220) of the matrix of the nitrided layer.

it is considered that the decrease in surface hardness at higher nitriding temperature was due to the decrease in the microstrain induced in the matrix of the nitrided layer, which was caused by coarsening of nitride particles.

Moreover, M phase shift was caused by nitriding temperature. At the low nitriding temperature, M phase peaks were located at the lower angle than each Ni (γ) peak of the substrate base metal, but at the high nitriding temperature, these peaks shifted to a higher angle than Ni (γ). This suggests that the lattice parameter of M phase is changed by nitriding temperature. The reason M phase peaks locate at the lower diffraction angle than Ni (γ) is the expansion of M phase lattice owing to dissolving a lot of nitrogen atoms into the matrix of the nitrided layer as a solid solution. In addition, in this case, the precipitated particles in the nitrided layer should have the coherency with the matrix like metastalbe particles as GP zone.[8,9] Similar phenomena of the expanding lattice of the matrix of the nitrided layer was reported in the nitrided Mo-Ti,[10] Fe-Ti,[11] Fe-Cr, Fe-V, and Fe-Mo alloys.[12]

On the contrary, at the high nitriding temperature, precipitated particles were equilibrium nitride phase without coherency with the matrix of the nitrided layer. The alloying element in the matrix was exhausted by the formation of the nitrides. Thus, the shifting of M phase peak at high nitriding temperature was caused by the depletion of alloying content in the matrix of the nitrided layer as well as the decrease in solution nitrogen content.

F. *Hardening Mechanism of Ni Alloys by Plasma Nitriding*

Figures 18 and 19 show the effect of nitride particle density and particle size on the surface hardness and half value width of the diffraction peak of the matrix of the nitrided layer, M peak at nitriding temperature range 823 to 1073 K. Surface hardness and half value width of M peak increased linearly with increasing particle density and decreasing particle size. Namely, these results reveal that high precipitation density of fine coherent particles induced the large microstrain in the matrix of the nitrided layer and this caused the hardening of the nitrided layer. Based on the results, it is considered that the hardness decrease at high nitriding temperature was owing to the decrease of this microstrain, which was caused by the coarsening of nitride and the decrease of precipitation density.

Accordingly, the hardening mechanisms of Ni alloys by plasma nitriding are drawn schematically as Figure 20. At the first stage of plasma nitriding, nitrogen diffuses into the Ni alloy, and combines with the alloying element to form the nitride or the metastable precipitates as the internal nitriding process.[13]

In the case of lower nitriding temperature, a lot of nitrogen was dissolved in the matrix of the nitrided layer, and the fine metastable particle or GP zone, which has coherence with the matrix of the nitrided layer, is formed. These fine particles induce the large microstrain in the matrix and this causes the hardening of the nitrided layer. On the contrary, in the case of higher nitriding temperature, nitrogen was combined with the alloying element and formed the stable and large nitrides in the nitrided layer. They have, however, no coherence with the matrix, thus, the hardness of the

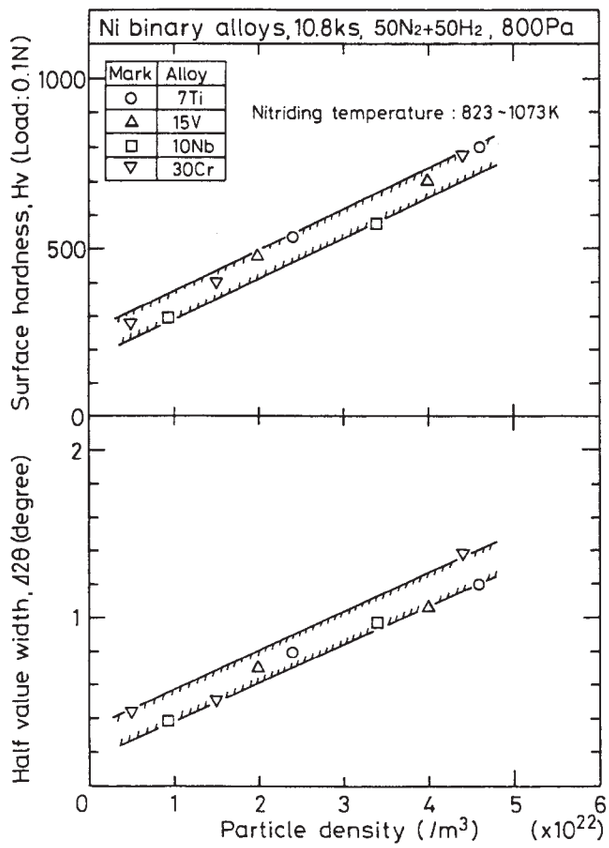

Fig. 18—Effect of nitride particle density on the surface hardness and half value width of XRD (220) of the matrix of the nitrided layer.

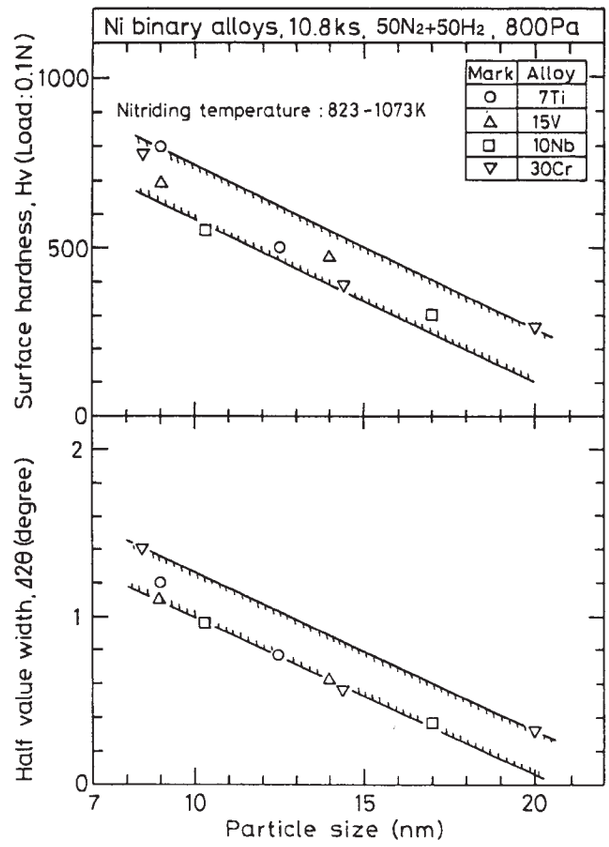

Fig. 19—Effect of nitride particle size on the surface hardness and half value width of XRD (220) of the matrix of the nitrided layer.

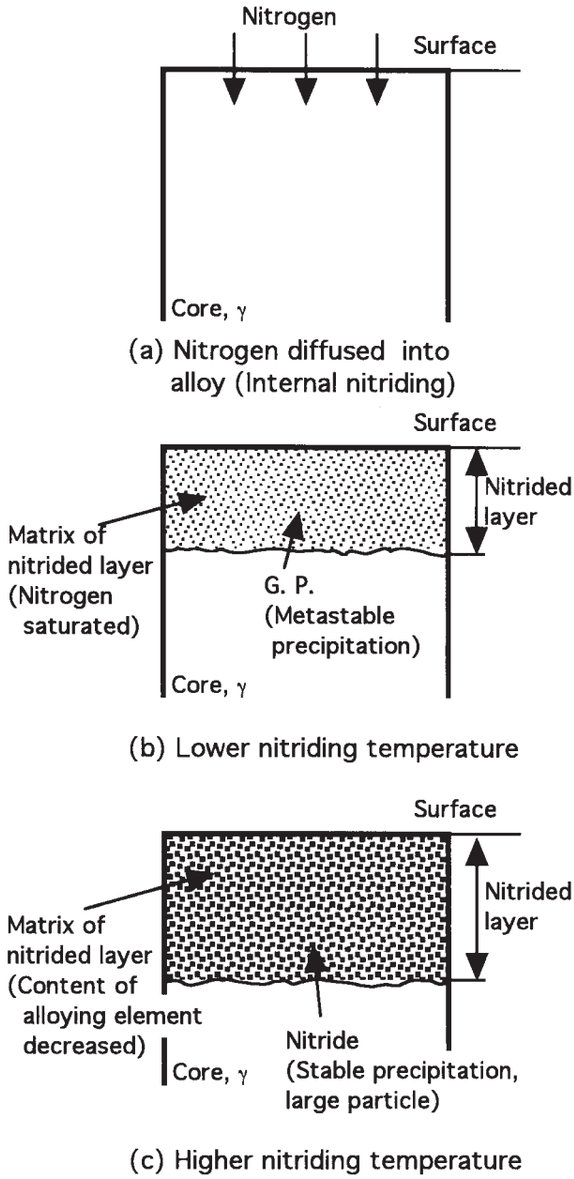

Fig. 20—(*a*) through (*c*) Schematic illustration showing the structure of the nitrided layer and the hardening mechanism of Ni alloys at different nitriding temperatures of plasma nitriding.

nitrided layer at high nitriding temperature is lower than that at the low nitriding temperature.

Therefore, it is made clear that the surface hardening of Ni alloys by plasma nitriding is due to the microstrain induced in the matrix of the nitrided layer caused by the formation of fine precipitation particles having coherence with the matrix.

IV. CONCLUSIONS

Surface hardening of Ni alloys by plasma nitriding was investigated by using 31 types of tentative Ni binary alloys contained a nitride forming element at the nitriding temperature range from 673 to 1073 K. As a result, the following conclusions were obtained.

1. All tentative Ni binary alloys containing Ti, Zr, Hf, V, Nb, Ta, Cr, Mo, Mn, Fe, Al, or Si were hardened by plasma nitriding. Surface hardness was different from depending on the types of alloying elements and their contents. A higher hardness than HV500 was obtained in Ti, V, Nb, and Cr containing alloys, but other alloys showed a lower surface hardness than HV400.
2. Surface hardness was increased linearly with the alloying content. The hardness increase rate for alloying content was classified as followed: Ti > (V, Nb, Ta) > (Al, Cr, Mo, Si) > (Mn, Fe). The Ti, V, Nb, and Cr were the effective alloying elements for the surface hardening of Ni alloys by plasma nitriding. The others were not effective due to the low hardness increase rate or low solubility in nickel.
3. By using the hardness increasing rate for alloying content, an equation to estimate the surface hardness of Ni alloys was drawn. The applicability of this equation was confirmed by estimating the surface hardness of commercially used Ni alloy after plasma nitriding.
4. A nitrided layer was observed in Ni-Ti, -V, -Nb, and -Cr alloys, which showed remarkable surface hardening. The Ni-Ti alloys formed the thickest nitrided layer among all Ni alloys used.
5. The nitrided layer was composed of fine precipitate particles in the matrix of the nitrided layer. In the case of lower nitriding temperature, these particles were metastable fine particles or GP zone having coherency with the matrix, and these fine particles induced large microstrain in the matrix of the nitrided layer. In higher nitriding temperature, equilibrium nitride particles, TiN, VN, NbN, and CrN, for each alloy were precipitated and coherency with the matrix was decreased. The particle size increased with increasing nitriding temperature from about 6 to 20 nm, and the particle precipitation density decreased with increasing nitriding temperature.
6. Diffraction peaks of the nitride and the matrix of the nitrided layer in Ni-Ti, -V, -Nb, and -Cr alloys were very broad. This broadening was induced by the precipitation of coherent particles, and the half value width of the peak from the matrix of the nitrided layer, which represented the broadening, increased linearly with increasing particle precipitation density and decreased linearly with increasing size of the particle.
7. The surface hardness of the nitrided layer had a close relationship with the half value width of the peak from the matrix of the nitrided layer, and increased linearly with the increasing half value width. This strongly suggested that the hardening of Ni alloys by plasma nitriding was due to the microstrain induced in the nitrided layer by the precipitation of metastable particle or GP zone.

ACKNOWLEDGMENTS

The author thanks F. Matsuda, Emeritus Professor, Osaka University, for his supervision and discussions, and Sumitomo Metal Industries Ltd. for supplying tentative Ni alloys.

REFERENCES

1. F. Matsuda, K. Nakata, and K. Tohmoto: *Trans. JWRI,* 1983, vol. 11, pp. 97-104.
2. B. Edenhofer: *Heat Treatment Met.,* 1975, vol. 30, pp. 204-08.

3. M. Liu: *High Temp. Sci.,* 1978, vol. 10, pp. 53-65.
4. M. Hansen: *Constitution of Binary Alloys,* McGraw-Hill Book Co., New York, NY, 1958.
5. P.B. Hirsch, A. Howie, R. B. Nicholson, D.W. Pashley, and M.J. Whelan: *Electron Microscopy of Thin Crystals,* Corona Publishing Co. Ltd., Tokyo, Japan, 1969, pp. 170-77 (in Japanese).
6. E.T. Turkdugan: *Physical Chemistry of High Temperature Technology,* Academic Press, New York, NY, 1980, pp. 1-24.
7. E.J. Mittemeijer: *J. Met.,* 1985, vol. 9, pp. 16-20.
8. A. Krowitz and R. Sinelair: *Phil. Mag.,* 1975, vol. 31, pp. 697-712.
9. K.H. Jack: *Proc. Heat Treatment '73,* The Metals Society, London, 1975, pp. 39-51.
10. S. Yano, S. Morozumi, and S. Koda: *Scripta Metall.,* 1978, vol. 12, pp. 467-70.
11. D.H. Jack: *Acta Metall.,* 1976, vol. 24, pp. 137-46.
12. M.A.J. Somers, R.M. Lankreijer, and E.J. Mittemeijer: *Phil. Mag.,* 1989, vol. 59, pp. 353-78.
13. D.J. Iden and L. Himmel: *Acta Metall.,* 1969, vol. 17, pp. 1483-99.